Jin et al. J Nanobiotechnol (2019) 17:99
https://doi.org/10.1186/s12951-019-0532-9

Journal of Nanobiotechnology

RESEARCH Open Access

Hollow gold nanoshells-incorporated injectable genetically engineered hydrogel for sustained chemo-photothermal therapy of tumor

RuiMei Jin[1†], Jie Yang[1†], DongHui Zhao[1], XiaoLin Hou[1], ChaoQing Li[1], Wei Chen[1], YuanDi Zhao[1,2], ZhongYuan Yin[3*] and Bo Liu[1,2*]

Abstract

Background: Combined therapy has demonstrated to be an effective strategy for cancer therapy. Herein, an injectable hydrogel based on the genetically engineered polypeptide and hollow gold nanoshells (HAuNS) has been developed for chemo-photothermal therapy of HepG2 tumor.

Methods: $PC_{10}A$/DOX/HAuNS nanogel was prepared with layer-by-layer through the adsorption of DOX and $PC_{10}A$ successively. DOX with positive charge and $PC_{10}A$ with negative charge were coated step by step onto the surface of negatively charged HAuNS. The multifunctional hydrogel $PC_{10}A$/DOX/HAuNS were prepared via dissolving hybrid $PC_{10}A$/DOX/HAuNS nanogel in polypeptide $PC_{10}A$. Chemotherapy drug DOX in the $PC_{10}A$/DOX/HAuNS hydrogel was absorbed on the HAuNS and directly embedded in the $PC_{10}A$ hydrogel, which contributes to sequentially release of the drug. Specifically, DOX adsorbed on the HAuNS could be released slowly for sustainable chemotherapy.

Results: The $PC_{10}A$/DOX/HAuNS hydrogel could pass 26-gauge needle without clogging, indicating that it is injectable. In addition, the $PC_{10}A$/DOX/HAuNS hydrogel possessed outstanding photothermal effect and photothermal stability. In both in vitro cell and in vivo tumor-bearing mice experiments, a remarkably enhance tumor inhibition was observed by the combined therapy of chemo-photothermal therapy compared with photothermal therapy or chemotherapy alone.

Conclusions: The combined chemotherapy and photothermal therapy of $PC_{10}A$/DOX/HAuNS hydrogels could significantly improve the therapeutic effect. Therefore, the multifunctional hydrogel $PC_{10}A$/DOX/HAuNS is promising to provide a new strategy for sustained chemo-photothermal therapy.

Keywords: Injectable hydrogel, Hollow gold nanoshells, Genetically engineered polypeptide, Chemotherapy, Photothermal therapy

*Correspondence: yzyunion@163.com; lbyang@mail.hust.edu.cn
†RuiMei Jin and Jie Yang contributed equally to this article
[2] Key Laboratory of Biomedical Photonics (HUST), Ministry of Education, Huazhong University of Science and Technology, Wuhan 430074, Hubei, People's Republic of China
[3] Cancer Center, Union Hospital, Tongji Medical College, Huazhong University of Science and Technology, Wuhan 430022, Hubei, People's Republic of China
Full list of author information is available at the end of the article

Introduction

Photothermal therapy (PTT), especially caused by near-infrared (NIR) light, has attracted lots of interest in tumor therapy owing to its deep tissue penetrability, non-radiative conversion of light energy, and specific spatial/temporal selectivity [1–3]. Various inorganic/organic nanomaterials, such as gold nanorod, hollow gold nanoshells (HAuNS), carbon tube, and indocyanine green were utilized as photothermal agents for PPT of tumors [4–7]. They are endowed with excellent light-to-heat conversion efficiency. For example, Chen et al. used $MoSe_2$ nanosheet for effectively CT26 colorectal tumor therapy [8]. Among them, HAuNS was most widely used due to its lack of need for cytotoxic surfactant, tremendous drug load capacity, and excellent photothermal efficiency [9–12]. However, PTT alone could not ablate completely the tumor cells due to residual tumor mass at the treatment margins, which easily result in tumor recurrence [13]. Therefore, combination strategies are expected to improve the overall efficacy of tumor treatment.

Chemotherapy is the traditional malignant tumor cure method in clinical application, while high dose chemotherapeutic drug administration was usually implemented to maintain the therapeutic drug concentration at the expense of serious side effects to normal tissue cells [14–16]. Since the last decade, anticancer drugs have been incorporated easily into the hydrogel for local chemotherapy, which avoided the long journey in the circulatory system, decreased toxicity to normal tissues [17–21]. Especially, injectable hydrogels can be used as drug carriers to provide drug directly located at the desired position in high-concentrations and leading to improved utilization efficiency [22–24]. Days or even weeks of continuous drug release of injectable hydrogel can avoid the side effects of multiple administration. In addition, different functional anticancer drugs and functional nanomaterials can be loaded in the injectable hydrogel by a simple mixture for sequential release and combined therapy [25, 26]. To date, injectable hydrogels are mostly synthetic polymer or natural proteins [27]. However, the potential toxicity of synthetic polymer and the complex composition of natural proteins limit their materials as drug delivery carriers [28]. Genetically engineered polypeptides with single component and high biocompatibility are very favorable to prepare injectable hydrogels as drug delivery carriers [29]. Previous studies have shown that HAuNS were widely used in the combined treatment of tumors due to their strong photothermal effect and high drug loading capacity [30]. However, the clinical applications of HAuNS alone for tumor therapy still face many challenges due to drug leakage and unstability under physiological conditions [31]. To overcome these limitations, the strategy with combination of HAuNS and polypeptide hydrogel is expected to achieve a satisfactory treatment outcome for tumor therapy.

Herein, we developed an injectable hydrogel based on the genetically engineered polypeptide and HAuNS for chemo-photothermal therapy of HepG2 tumor. We first prepared a drug-loaded hybrid $PC_{10}A$/DOX/HAuNS nanogel through layer-by-layer coating with DOX and $PC_{10}A$. The hybrid $PC_{10}A$/DOX/HAuNS nanogels were dissolved in $PC_{10}A$ hydrogel to product injectable $PC_{10}A$/DOX/HAuNS hydrogel exhibiting a variety of excellent functions (Scheme 1). One part of the drug DOX in the $PC_{10}A$/DOX/HAuNS hydrogel was absorbed on the HAuNS, and the other part was directly embedded in the $PC_{10}A$ hydrogel, which contributes to sequentially release of the drug. The $PC_{10}A$/DOX/HAuNS hydrogel had outstanding photothermal effect and photothermal stability. The results of toxicity showed that the $PC_{10}A$/DOX/HAuNS hydrogel presented excellent biocompatibility. The results of in vivo experiments have demonstrated that the combination of photothermal therapy and chemotherapy of $PC_{10}A$/DOX/HAuNS hydrogel exhibited a good inhibitory effect on HepG2 tumor, and the recurrence was controlled at a low level.

Materials and methods

Materials

Restriction endonuclease *Bam*HI, *Nhe*I, *Spe*I, and T4 DNA ligase were obtained from New England Biolabs Inc. (Beijing, China). Ampicillin and kanamycin were purchased from Sinopharm Group Chemical Reagent Co., Ltd (Shanghai, China). Isopropyl-*β*-D-thiogalactoside (IPTG) and nickelnitrilotriacetic acid (Ni-NTA) separation column were purchased from Qiagen Co., Ltd (Shanghai, China). Cobalt chloride hexahydrate (99.99%), gold chloride trihydrate ($HAuCl_4 \cdot 3H_2O$), trisodium citrate dehydrate (> 99%), polyvinylpyrrolidone (PVP, MW: 55,000), sodium borohydride (99%), calcein AM, Propidium Iodide (PI), and Doxorubicin Hydrochloride (DOX) were obtained from Sigma-Aldrich, Inc. (USA). Ultrapure water (18.2 MΩ) purified by the Milli-Q system (Millipore, DE) was used to prepare all solutions.

Preparation of the genetically engineered polypeptide $PC_{10}A$, HAuNS nanoparticles, and $PC_{10}A$/DOX/HAuNS hydrogels

PQE9$PC_{10}A$ plasmid was a gift from Prof. David Tirrell at the California Institute of Technology, Pasadena, CA. The genetically engineered polypeptide $PC_{10}A$ was prepared according to our previously reported method [32, 33]. The purified polypeptides were analyzed on a Bruker Reflex III reflectron MALDI-TOF mass spectrometer (Bremen, Germany).

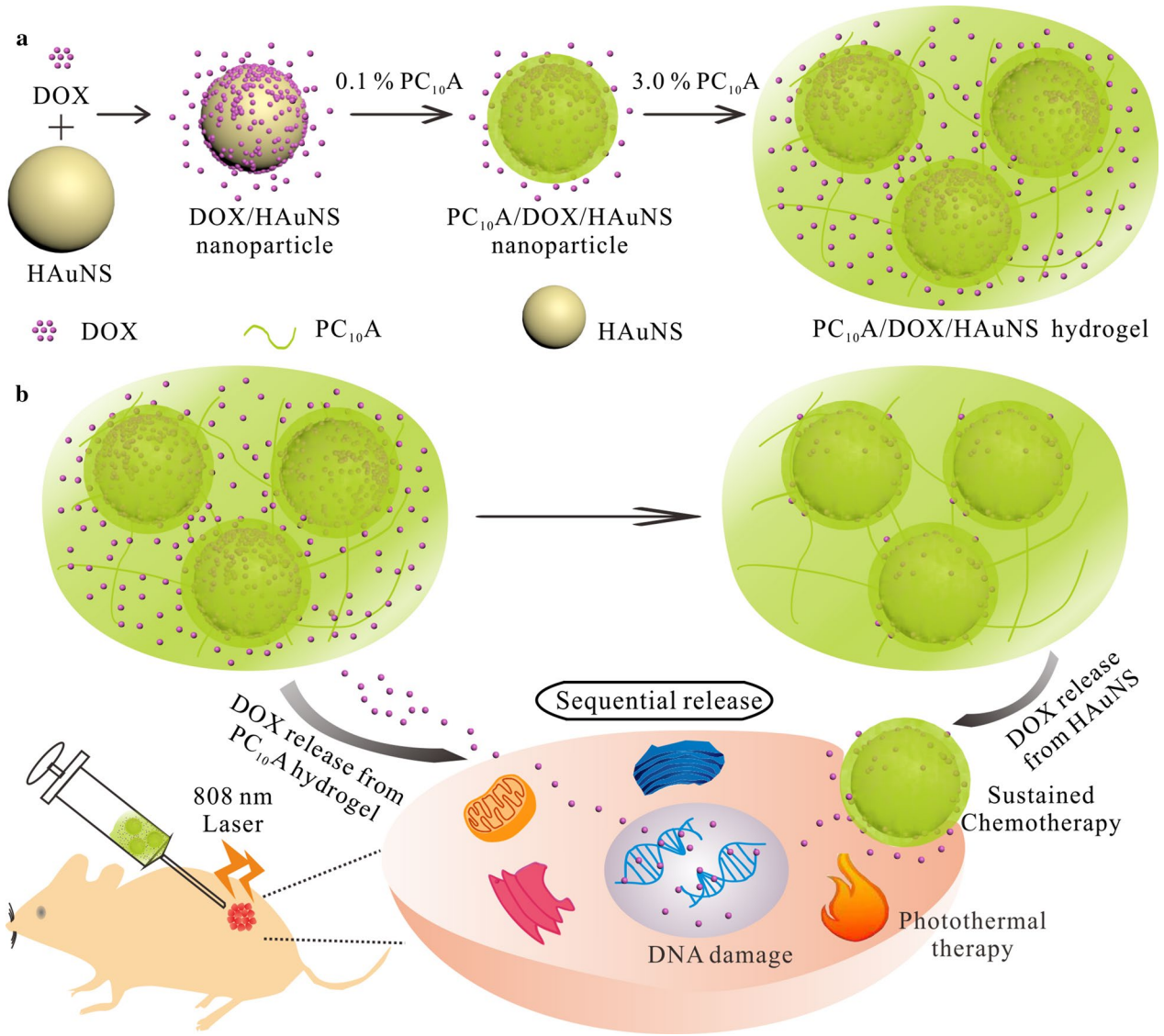

Scheme 1 **a** Schematic illustration of the preparation of $PC_{10}A$/DOX/HAuNS nanoparticles and $PC_{10}A$/DOX/HAuNS hydrogel through self-assemble layer-by-layer and "dissolving" the $PC_{10}A$/DOX/HAuNS nanoparticles in the $PC_{10}A$ hydrogel, respectively; **b** $PC_{10}A$/DOX/HAuNS hydrogel with sequential drug release were utilized for sustained chemotherapy and photothermal therapy in vivo

HAuNS nanoparticles were synthesized by the replacement of cobalt nanoparticles in the presence of chloroauric acid according to the method of Schwartzberg et al. [34]. Briefly, 0.1 mM $CoCl_2{\cdot}6H_2O$, 0.1 mM $C_6H_5Na_3O_7{\cdot}2H_2O$, and 10 μM PVP were dissolved in 100 mL water, stirred and protected with argon for 45 min. Eight hundred milliliters of 1 mM fresh sodium borohydride was added into the solution. The mixture was stirred for 60 min, and 430 μL $HAuCl_4{\cdot}3H_2O$ (1 g 100 mL^{-1}) was added into the mixture dropwise. The mixture was stirred for 25 min and exposed in the air until it turned to green. The mixture was centrifuged at 14,000 rpm for 20 min and washed with ultrapure water for three times. Five-hundred microliters of DOX solution (1.6 mg mL^{-1}) was dispersed into equal volume HAuNS nanoparticles solution (40 μg mL^{-1}). After stirring for 24 h, the mixture was repeated centrifugation (10,000 rpm, 20 min) to remove free DOX and obtain DOX-loaded HAuNS/DOX nanoparticle.

The quantity of unloaded DOX in the supernatant was estimated by the absorbance at 480 nm. The drug loading rate was calculated as follows: Drug Loading Rate = (mass of total DOX − mass of DOX in the supernatant)/mass of HAuNS/DOX × 100%.

One milligram $PC_{10}A$ was dissolved into above mixture to prepare $PC_{10}A$/DOX/HAuNS nanoparticles. Sizes of HAuNS nanoparticles, HAuNS/DOX nanoparticles and $PC_{10}A$/DOX/HAuNS nanoparticles were measured by a Tecnai G2 20 U-Twin TEM. Zeta potentials, hydrodynamic sizes, and UV–vis spectra of these nanoparticles were tested by a ZS90 electronic dynamic light scattering apparatus nanosizer (Malvern, U.K.) and a UV–vis spectrometer (Shimadzu, Japan), respectively.

Another 29 mg $PC_{10}A$ was dissolved in the $PC_{10}A$/DOX/HAuNS solution, and pH of the solution was adjusted to 7.4 to prepare the $PC_{10}A$/DOX/HAuNS hydrogel ($PC_{10}A$: 3% w/w, DOX: 0.8 mg mL^{-1}, HAuNS: 20 μg mL^{-1}). The $PC_{10}A$ hydrogel, $PC_{10}A$/DOX hydrogel, and $PC_{10}A$/HAuNS hydrogel were prepared by the same method. The morphology of lyophilized $PC_{10}A$ hydrogel, $PC_{10}A$/DOX hydrogel, $PC_{10}A$/HAuNS hydrogel, and $PC_{10}A$/HAuNS/DOX hydrogel was measured on a Nova Nano SEM 450 (FEI, USA).

Rheological tests of $PC_{10}A$ hydrogel and $PC_{10}A$/HAuNS/DOX hydrogel

The rheology properties of $PC_{10}A$/DOX/HAuNS hydrogel and blank $PC_{10}A$ hydrogel were carried out on a HR-2 hybrid rheometer (TA Instrument). $PC_{10}A$ ($PC_{10}A$: 3% w/w) and $PC_{10}A$/DOX/HAuNS hydrogel ($PC_{10}A$: 3% w/w, DOX: 0.8 mg mL^{-1}, HAuNS: 20 μg mL^{-1}) samples were mildly transferred into the middle of the 15 mm diameter parallel plate with a proper gap. Dynamic oscillatory frequency sweep measurements were conducted at the strain between 1% and 500%. Angular frequency dependent oscillatory rheology was tested from 10^{-2} to 10^{3} rad s^{-1}. Self-healing ability was measured by repeating dynamic strain of 1% and 500%. Viscosity test was operated at the shear rate between 1 and 10 s^{-1}. All the measurements were repeated for three times.

Photothermal effect of $PC_{10}A$/DOX/HAuNS hydrogel

Different concentrations of HAuNS nanoparticles (5, 10, 15, 20, 25 μg mL^{-1}) were exposed with an 808 nm (2.0 W cm^{-2}) laser for 9 min, and the temperatures were recorded by an EasIR-9 Thermal Imager (Wuhan Guide Infrared Co., Ltd, China). In addition, HAuNS solution (20 μg mL^{-1}) were irradiated with an 808 nm laser with different power densities (0.5, 1, 1.5, 2.0 and 2.5 W cm^{-2}), and the temperatures were also measured. Each experiment was repeated three times. The photothermal stability of HAuNS solution was measured by 6 circles laser irradiation on/off (λ = 808 nm, 2.0 W cm^{-2}). In addition, the photothermal effect of $PC_{10}A$ hydrogel, $PC_{10}A$/HAuNS hydrogel and $PC_{10}A$/DOX/HAuNS hydrogel were measured with the same method of HAuNS nanoparticles. The η value of HAuNS nanoparticles was calculated through previously reported method [35].

Cytotoxicity and hemolysis percentage of $PC_{10}A$/HAuNS hydrogel in vitro

HepG2 cells in DMEM (with 10% FBS) were seeded in 96-well plates (5000 cells per well) and cultured in a cell incubator (5% CO_2, 37 °C). After incubation for 20 h, the cells were washed with PBS and cultured with different concentrations of $PC_{10}A$ nanogel (0.8%, 0.4%, 0.2%, 0.1%, 0.05%) and HAuNS (HAuNS: 40, 20, 10, 5, 2.5 μg mL^{-1}) in serum-free DMEM for another 48 h. The variances of cells were measured through standard MTT assay.

The biocompatibility of $PC_{10}A$ hydrogels and $PC_{10}A$/HAuNS hydrogels were also tested by 3D cell culture. HepG2 cells (2×10^4 cells per milliliter hydrogel) were dispersed into $PC_{10}A$ hydrogel ($PC_{10}A$: 3% w/w) and $PC_{10}A$/HAuNS hydrogel ($PC_{10}A$: 3% w/w, HAuNS: 20 μg mL^{-1}) containing 100 units/mL penicillin and streptomycin, respectively. The cell-laden hydrogels were transferred into 35 mm glass bottom culture dishes and cultured at 37 °C under a humidified 5% CO_2 for 24 and 48 h. The cells were stained with the calcein AM and PI for 20 min and imaged with a 20× objective on an Olympus FLUOVIEW FV1000 confocal microscope (OLYMPUS, Japan).

One microliter of RBC was added on the $PC_{10}A$ hydrogel (200 μL, 3% w/w) and $PC_{10}A$/HAuNS hydrogel (200 μL; $PC_{10}A$: 3% w/w, HAuNS: 20 μg mL^{-1}), respectively. Equivalent PBS and water with RBC were set as controls. All of them were cultured at 37 °C for different times (2, 4, and 8 h). The mixture was centrifuged at 3500 rpm for 5 min, and the absorbance of supernatant was measured at 577 nm. The hemolysis ration was calculated by following equation: Hemolysis Ration = $(OD_{Sample} - OD_{PBS})/(OD_{Water} - OD_{PBS})$*100%, OD_{Sample}, OD_{PBS}, and OD_{Water} is the absorbance value of the corresponding supernatant at 577 nm.

Degradation of $PC_{10}A$/DOX/HAuNS hydrogel and DOX release

$PC_{10}A$ hydrogel (120 mg) was transferred into a cylindrical tube through centrifugation. PBS (3 mL) was added on the $PC_{10}A$ hydrogel, and the tube was incubated in 37 °C. The erosion profiles of $PC_{10}A$ hydrogel in the PBS were determined by measuring the absorbance at 278 nm at successive time points, and equal volume fresh PBS was replaced. In addition, DOX release from $PC_{10}A$/DOX/HAuNS hydrogel and $PC_{10}A$/DOX hydrogel was tested. The $PC_{10}A$/DOX/HAuNS hydrogel (0.5 mL) contained concentrated DOX/HAuNS (HAuNS: 20 μg mL^{-1}, DOX: 0.8 mg mL^{-1}) and $PC_{10}A$/DOX (DOX 0.8 mg mL^{-1}) were prepared and transferred into cylindrical tubes,

respectively. Equivalent volume of PBS buffer (pH 7.4) or acetate buffer (pH 5.0) was added on the hydrogels. At each time point, 0.5 mL buffer was taken out and replaced with an equivalent volume of fresh buffer. The release of DOX was detected by the measurement absorption spectra at 480 nm on a UV-2550 UV–vis spectrophotometer (Shimadzu, Japan).

Intratumoral retention and drug distribution in different organs

$PC_{10}A$/IR783 hydrogel ($PC_{10}A$: 3% w/w, IR783: 40 μg mL^{-1}) was prepared by the similar method described above. Two groups of HepG2 tumor-bearing mice were dividedly injected with 100 μL free IR783 solution and $PC_{10}A$/IR783 hydrogel with the same dose of IR783 (40 μg mL^{-1}) by intratumoral injection. The imaging experiments were performed using a home-built mouse image system equipped with an excitation band pass filter at 740 nm and an emission optical filter at 800 nm. On day 6, one mouse of each group sacrificed, the major organs and tumor were imaged on collected on the home-built fluorescence system.

Combination of chemotherapy and phototherapy in vitro and in vivo

HepG2 cells (20,000 cells per milliliter hydrogel) were dividedly embedded in blank $PC_{10}A$ hydrogel, $PC_{10}A$/HAuNS hydrogel, $PC_{10}A$/DOX hydrogel, and $PC_{10}A$/DOX/HAuNS hydrogel ($PC_{10}A$: 3%, HAuNS: 20 μg mL^{-1}, DOX: 0.8 mg mL^{-1}) and cultured for 24 h. Cells in blank $PC_{10}A$ hydrogel, $PC_{10}A$/HAuNS hydrogel hydrogel, and $PC_{10}A$/DOX/HAuNS hydrogel were irradiated with an 808 nm laser at a power density of 2.0 W cm^{-2} for 9 min. Following, the cells were stained with calcein AM and PI and imaged with a 20× objective on an Olympus FLUOVIEW FV1000 confocal microscope (OLYMPUS, Japan).

In addition, the photothermal efficiency of $PC_{10}A$/DOX/HAuNS hydrogel in vivo was tested. One hundred microliter $PC_{10}A$/DOX/HAuNS hydrogel ($PC_{10}A$: 3% w/w, HAuNS: 20 μg mL^{-1}, DOX: 0.8 mg mL^{-1}) and blank $PC_{10}A$ hydrogel ($PC_{10}A$: 3%) were separately injected into two groups of HepG2 tumor-bearing mice by intratumoral injection. All the tumors were irradiated under an 808 nm laser at the density of 2.0 W cm^{-2} for 9 min, and the temperature changes were recorded by an EasIR-9 Thermal Imager.

Forty-two HepG2 tumors-bearing male mice with the average tumor size ranging from 100 to 150 mm^3 were randomly separated to seven groups, namely: (1) PBS group, (2) laser alone group, (3) $PC_{10}A$ group, (4) Free DOX group, (5) $PC_{10}A$/DOX hydrogel group, (6) $PC_{10}A$/HAuNS (laser+) hydrogel group, and (7) $PC_{10}A$/DOX/HAuNS (laser+) hydrogel group (n = 7). One hundred microliter PBS, $PC_{10}A$ hydrogel, $PC_{10}A$/HAuNS hydrogel, free DOX solution, $PC_{10}A$/DOX hydrogel, and $PC_{10}A$/DOX/HAuNS hydrogel ($PC_{10}A$: 3% w/v, HAuNS: 20 μg mL^{-1}, DOX: 0.8 mg/mL) was injected into the tumor, respectively. Mice of the laser alone group, $PC_{10}A$/HAuNS group, and $PC_{10}A$/DOX/HAuNS group were treated with laser irradiation (808 nm, 2 W cm^{-2}) for 9 min. One tumor of each group was harvested after treatment for 24 h to H&E stain. The tumor sizes and body weights were recorded during the cure process. At the end of the cure, all the mice were sacrificed for the major organs and blood samples used for H&E stain and blood analysis.

Long-term tumor therapy efficiency and recurrence rate

Fifteen HepG2 tumor-bearing male mice were randomly divided into three groups (n = 5) to study long-term therapy efficiency and recurrence rate of $PC_{10}A$/DOX/HAuNS hydrogel. Mice were injected with $PC_{10}A$/DOX hydrogel, $PC_{10}A$/HAuNS hydrogel, and $PC_{10}A$/DOX/HAuNS hydrogel by intratumoral injection. Except for the $PC_{10}A$/DOX group, all the other tumors were treated with laser irradiation (808 nm, 2 W cm^{-2}) for 10 min. On day 72, one tumor in the $PC_{10}A$/DOX/HAuNS hydrogels group was dissected to inspect the residual hydrogel. The cure course was continued for 72 days. Tumors were divided and made photograph at the end of the cure. Survival percent was recorded during this course.

Results and discussion

Characterization of multifunctional $PC_{10}A$/DOX/HAuNS hydrogel

A triblock genetically engineered polypeptide $PC_{10}A$ containing two coiled-coil domains P and A, which were located in the two terminals of the polypeptide, and a soluble random coil midblock C_{10} were prepared according to our previously reported method [32, 33]. The mass of the polypeptide $PC_{10}A$ was analyzed by a Bruker Reflex III reflectron MALDI-TOF mass spectrometer. $PC_{10}A$ (MS: 20,932.6 Da, the theoretical calculation of molecular weight: 20,858.5 Da). In addition, HAuNS with maximum absorption peak of 782 nm were synthesized through the method reported by Schwartzberg [34]. TEM images showed that HAuNS were homogenous with the diameter about 37.65 ± 4.23 nm (Fig. 1a). The different orientate lattice spaces with the gap about 0.20 nm and 0.24 nm agreed with the (111) and (200) crystal face, respectively, proving that HAuNS possessed the significant polycrystalline structure (Fig. 1b). To construct the multifunctional $PC_{10}A$/DOX/HAuNS hydrogel, hybrid $PC_{10}A$/DOX/HAuNS nanoparticles were prepared first. DOX with positive charge and $PC_{10}A$

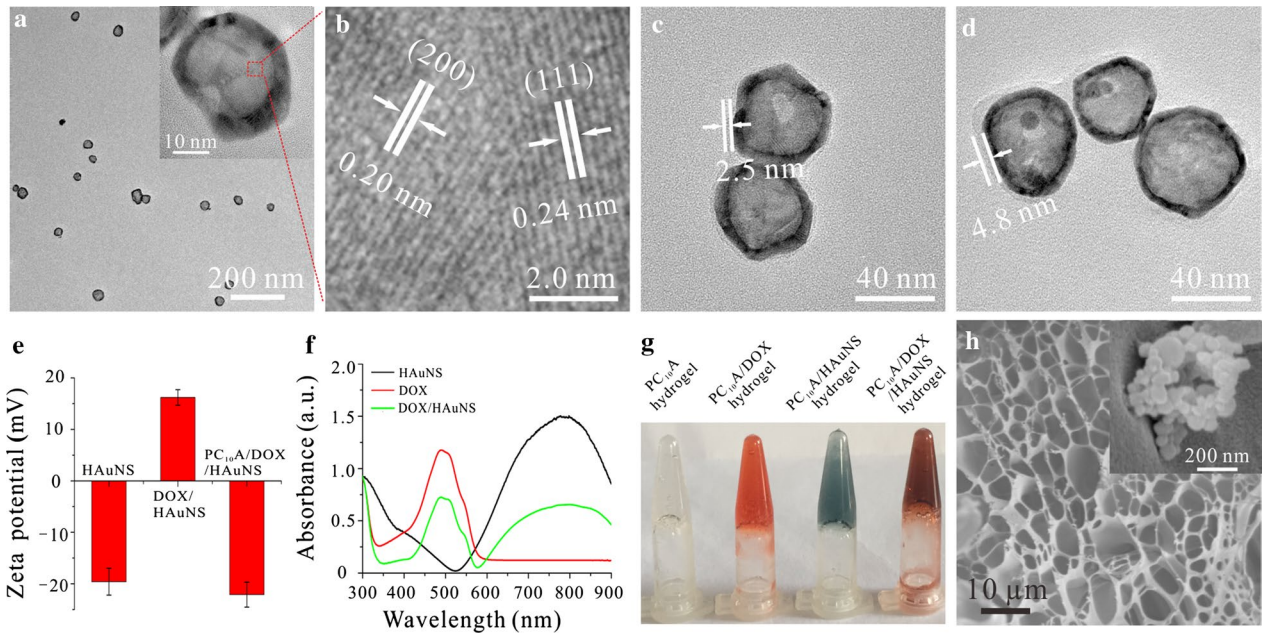

Fig. 1 Characterization of $PC_{10}A$/DOX/HAuNS nanogels and $PC_{10}A$/DOX/HAuNS hydrogels. **a** TEM image and high resolution TEM image (insert) of HAuNS; **b** the different orientate lattice of HAuNS; TEM image of HAuNS/DOX nanoparticles (**c**) and $PC_{10}A$/DOX/HAuNS nanoparticles (**d**); **e** zeta potentials of HAuNS, DOX/HAuNS nanoparticles, and $PC_{10}A$/DOX/HAuNS nanoparticles; **f** UV–vis absorbance spectra of HAuNS solution, DOX solution, and DOX/HAuNS solution; **g** photographs of $PC_{10}A$ hydrogel, $PC_{10}A$/DOX hydrogel, $PC_{10}A$/HAuNS hydrogel, and $PC_{10}A$/DOX/HAuNS hydrogel ($PC_{10}A$: 3% w/w, DOX: 0.8 mg mL^{-1}, HAuNS: 20 μg mL^{-1}); **h** SEM image and the high resolution SEM (insert) of the $PC_{10}A$/DOX/HAuNS hydrogel

with negative charge were coated step by step onto the surface of negatively charged HAuNS nanoparticles to prepare the hybrid $PC_{10}A$/DOX/HAuNS nanoparticles. Compared to the HAuNS nanoparticles, an obviously DOX layer with thickness about 2.5 nm could be seen on the surface of DOX/HAuNS nanoparticles (Fig. 1c). In addition, the coating layer of the HAuNS nanoparticles after modifying with $PC_{10}A$ increased to 4.8 nm (Fig. 1d), which may attribute to the second coating of $PC_{10}A$ polypeptide on the out layer of DOX/HAuNS. The results of dynamic light scattering analysis showed that the hydrodynamic sizes of HAuNS, DOX/HAuNS, and $PC_{10}A$/DOX/HAuNS increased gradually (Additional file 1: Fig. S1), which was consistent with those of TEM images. To further confirm that the hybrid $PC_{10}A$/DOX/HAuNS nanoparticles were formed by electrostatic adsorption layer-by-layer, the zeta potentials of HAuNS, DOX/HAuNS, and $PC_{10}A$/DOX/HAuNS were measured (Fig. 1e). The surface charges of DOX/HAuNS changed from negative (−19.6 mV) to positive (+16.2 mV) because of positively charged DOX, indicating that DOX was successfully coated on the surface of HAuNS. While HAuNS coated with DOX followed by a layer of negatively charged $PC_{10}A$ exhibited negative charge (−22.2 mV). These results demonstrated that hybrid $PC_{10}A$/DOX/HAuNS nanoparticles were self-assembled layer-by-layer through the electrostatic adsorption. Compared with the absorption spectra of DOX and HAuNS, the characteristic absorption peak of DOX at 480 nm and the localized surface plasmon resonance peak of HAuNS at 782 nm were observed in the absorption spectrum of HAuNS/DOX (Fig. 1f), further indicating that DOX was successfully coated on the surface of HAuNS. Previous studies showed that $PC_{10}A$ could form stable physical hydrogel through self-assemble when its concentration was above 2% (w/w). Hybrid $PC_{10}A$/DOX/HAuNS hydrogels were prepared through "dissolving" the $PC_{10}A$/DOX/HAuNS nanoparticles in the $PC_{10}A$ hydrogel because they both contained the same composition $PC_{10}A$ (Fig. 1g). SEM image showed that the $PC_{10}A$/DOX/HAuNS hydrogel was composed of a regular fiber framework and displayed highly porous interconnected structure (Fig. 1h). The HAuNS nanoparticle could be observed in the hydrogel in the high resolution SEM image (Fig. 1h, insert, Additional file 1: Fig. S2). No obvious difference of morphology was observed between blank $PC_{10}A$ hydrogel, $PC_{10}A$/DOX hydrogel, $PC_{10}A$/HAuNS hydrogel, and $PC_{10}A$/DOX/HAuNS hydrogel (Additional file 1: Fig. S3), their diameters of the pore crossed by skeleton were about 10 ± 5 μm, indicating that

the addition of DOX and HAuNS did not affect the structures of these hydrogels.

Rheological behaviors of $PC_{10}A$/DOX/HAuNS hydrogel

To characterize the viscoelastic properties of the $PC_{10}A$/DOX/HAuNS hydrogel, rheology experiments of $PC_{10}A$ hydrogels and $PC_{10}A$/DOX/HAuNS hydrogels were tested on a DHR-2 rheometer. Both hydrogels possessed similar viscoelastic features (Fig. 2a). Under the strain of 1–100%, storage moduli (G′) values of $PC_{10}A$ hydrogels and $PC_{10}A$/DOX/HAuNS hydrogels were five times bigger than that of loss moduli (G″) at the angular frequency of 6.28 rad/s. This result indicated that both $PC_{10}A$ hydrogels and $PC_{10}A$/DOX/HAuNS hydrogels exhibited linear viscoelastic behavior. With the further increase of strain, the sharp decrease of G′ and the gradual increase of G″ resulted in G′ < G″. When the strain was beyond 300%, $PC_{10}A$ hydrogels and $PC_{10}A$/DOX/HAuNS hydrogels displayed nonlinear viscoelastic behavior. These results suggested that these hydrogels were physical hydrogels [36, 37]. Angular frequency dependent oscillatory rheology experiment was also performed (Fig. 2b). G′ increased along with the angular frequency from 0.01 to 100 rad s^{-1}. While G″ trended to decrease after the angular frequency came to 0.06 rad/s. The cross point between G′ and G″ implied the phase transformation moment. When the HAuNS nanoparticles were incorporated into the $PC_{10}A$ hydrogel (3% w/w), the G′ of hydrogel increased from 134 to 178 Pa, indicating that the strength of $PC_{10}A$ hydrogel could be tuned by the addition of HAuNS nanoparticles. This result is probably due to the fact that HAuNS in the hydrogel can act as cross-linkers in the hydrogel. Continuous changing strain between 500% and 1% at the same frequency (6.28 rad s^{-1}) was performed to assess the strain-induced damage and self-healing ability of these hydrogels (Fig. 2c). G′ and G″ remained stable after 3 cycles of breaking and reforming, supporting that these hydrogels possessed favourable self-healing properties. In addition, a continuous flow experiment with the shear rate ranging from 1 to 10 s^{-1} under the constant strain of 1% was operated (Fig. 2d). The viscosity decreased with the increase of shear rate, indicating that

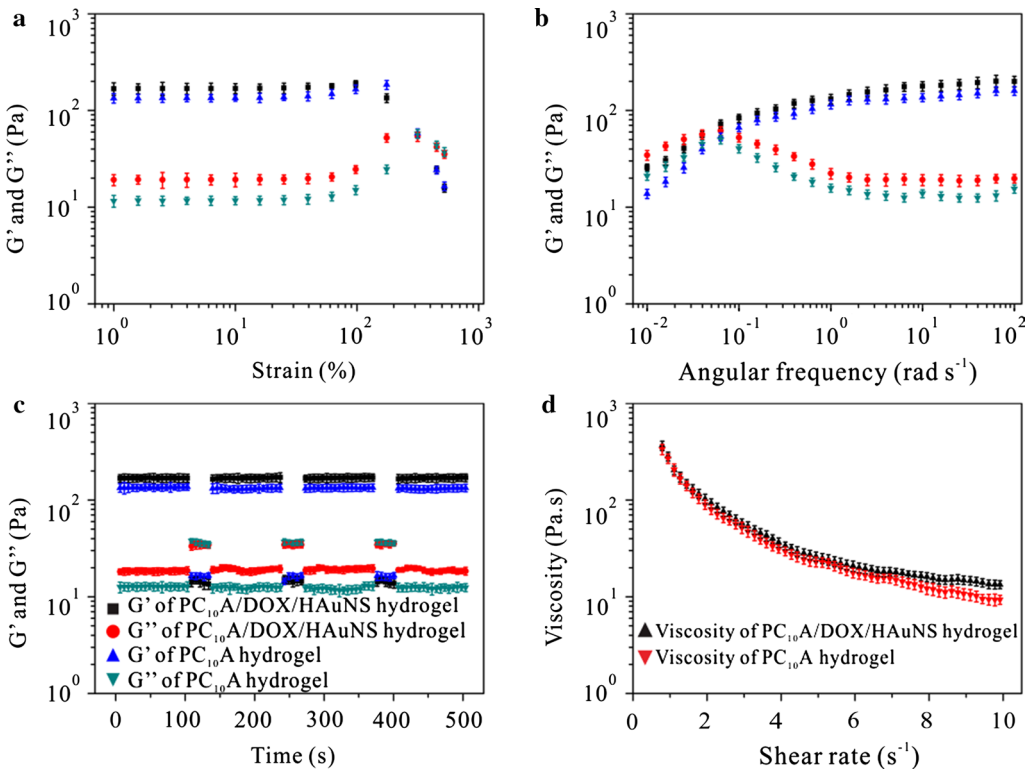

Fig. 2 Rheological characterizations of $PC_{10}A$ hydrogels and $PC_{10}A$/DOX/HAuNS hydrogels. **a** Dynamic oscillatory frequency sweep measurement (ω = 6.28 rad s^{-1}) and **b** frequency dependent (strain = 1%) oscillatory shear rheology of the 3% w/w $PC_{10}A$ hydrogel and $PC_{10}A$/DOX/HAuNS hydrogel ($PC_{10}A$: 3% w/w, DOX: 0.8 mg mL^{-1}, HAuNS: 20 μg mL^{-1}); **c** the self-repairing properties of the $PC_{10}A$ hydrogel and $PC_{10}A$/DOX/HAuNS hydrogel ($PC_{10}A$: 3% w/w, DOX: 0.8 mg mL^{-1}, HAuNS: 20 μg mL^{-1}) demonstrated by the step-strain tests at an alternative strain of 1% and 500%; **d** viscosity curve of the 3% w/w $PC_{10}A$ hydrogel and $PC_{10}A$/DOX/HAuNS hydrogel ($PC_{10}A$: 3% w/w, DOX: 0.8 mg mL^{-1}, HAuNS: 20 μg mL^{-1}). n = 3

these hydrogels presented considerable shear-thinning property. This property is the basis for the injectable ability of hydrogels [38]. No obvious difference between the two viscosity curves of $PC_{10}A$ hydrogel and $PC_{10}A$/DOX/HAuNS hydrogel was observed, suggesting that the addition of HAuNS nanoparticle and DOX had little effect on the viscosity of $PC_{10}A$ hydrogel. Excitingly, $PC_{10}A$/DOX/HAuNS hybrid hydrogel could be transferred into the syringe and pass a 26-gauge needle without clogging (Additional file 1: Fig. S4), which was consistent with the result of viscosity test. Therefore, the $PC_{10}A$/DOX/HAuNS hydrogel was expected to be used as an injectable carrier for tumor therapy.

Photothermal effect of $PC_{10}A$/DOX/HAuNS hydrogel

The photothermal conversion ability of photothermal agents plays an important role in photothermal therapy. To evaluate the photothermal effect of HAuNS nanoparticles in the $PC_{10}A$/DOX/HAuNS hydrogel, different concentrations of HAuNS were exposed with an 808 nm laser (2.0 W cm^{-2}). Temperatures of HAuNS solution increased quickly and eventually reached a plateau within 9 min (Fig. 3a), indicating that HAuNS can absorb the light and efficiently convert light energy to thermal energy. The photothermal effects of HAuNS solution under different laser power densities were also evaluated. The temperatures of HAuNS solution improved along with the increase of power density of the laser (Additional file 1: Fig. S5). These results exhibited that the temperature rising rates and the final temperature of the HAuNS solution under laser irradiation were depended on the concentration of HAuNS and the density of the laser.

Subsequently, photothermal stability of HAuNS nanoparticles was examined. HAuNS were exposed under the laser irradiation for 9 min and cooled it down at room temperature (Fig. 3b). After six cycles of laser irradiation, no obvious difference of the temperature change curve was observed. This result clarified that HAuNS nanoparticles presented outstanding photothermal stability. The photothermal effect of $PC_{10}A$ hydrogel, $PC_{10}A$/HAuNS hydrogel, and $PC_{10}A$/DOX/HAuNS hydrogel were also

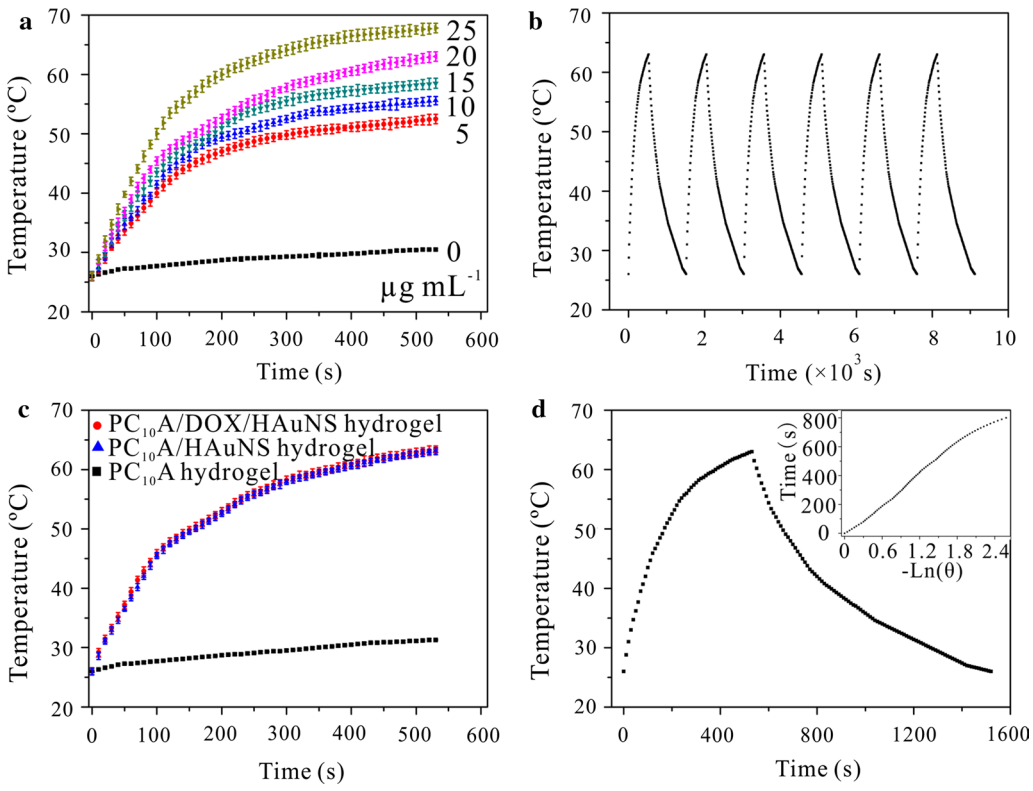

Fig. 3 Photothermal characterizations of $PC_{10}A$/DOX/HAuNS hydrogels. **a** Temperature changes of $PC_{10}A$/DOX/HAuNS nanogels ($PC_{10}A$: 0.1% w/w, DOX: 0.8 mg mL^{-1}) containing different concentrations of HAuNS (25, 20, 15, 10, 5, and 0 μg mL^{-1}) under irradiation with an 808 nm laser for 9 min (2.0 W cm^{-2}); **b** photothermal stability of the HAuNS under six irradiation on/off cycles (808 nm, 2.0 W cm^{-2}); **c** temperature changes of the $PC_{10}A$ hydrogel, $PC_{10}A$/HAuNS hydrogel, and $PC_{10}A$/DOX/HAuNS hydrogel ($PC_{10}A$: 3% w/w, DOX: 0.8 mg mL^{-1}, HAuNS: 20 μg mL^{-1}) under irradiation (2.0 W cm^{-2}) with an 808 nm laser for 9 min; **d** temperature changes of the $PC_{10}A$/DOX/HAuNS nanogel ($PC_{10}A$: 0.1% w/w, DOX: 0.8 mg mL^{-1}, HAuNS: 20 μg mL^{-1}) under laser irradiation (808 nm, 2.0 W cm^{-2}) for 9 min and cooling for 16 min. n = 3

investigated. The temperature increasing trend of $PC_{10}A$/HAuNS hydrogel and $PC_{10}A$/DOX/HAuNS hydrogel was the same as those of HAuNS nanoparticles with the same concentration (Fig. 3a, c), while the increased temperatures of $PC_{10}A$ hydrogel were nearly negligible. These results indicated that HAuNS nanoparticles in the $PC_{10}A$ hysdrogel still emerged prominent photothermal effect. $PC_{10}A$/HAuNS hydrogel and $PC_{10}A$/DOX/HAuNS hydrogel trended to flow state after irradiation with a laser, while it returned to gel state after cooling (Additional file 1: Fig. S6). It is probably because $PC_{10}A$ in the hydrogel is a thermosensitive polypeptide. This result further demonstrated that $PC_{10}A$ hydrogel was a reversible physical hydrogel in response to changes in temperature. A typical temperature versus time plot of HAuNS was obtained with the irradiation of 2.0 W cm^{-2} for 9 min and cooling down under room temperature (Fig. 3d). The η value of HAuNS nanoparticle was measured by Roper's method [35]. The value of η was 12.04%, indicating that HAuNS could use as an excellent photothermal agent for photothermal therapy of tumors.

Biocompatibility and hemolysis ration of $PC_{10}A$ hydrogel in vitro

To assess the biocompatibility of $PC_{10}A$/HAuNS hydrogels, the cell viabilities of HepG2 cells cultured with different concentrations of $PC_{10}A$ and HAuNS were tested by MTT assay. The cell viabilities of HepG2 cells were above 80% even the concentration of $PC_{10}A$ as high as 8 mg mL^{-1} or HAuNS as high as 20 μg mL^{-1} (Fig. 4a, b), which suggested that both $PC_{10}A$ and HAuNS were non-toxic to HepG2 cells. At the same time, the biocompatibility of $PC_{10}A$ hydrogel and $PC_{10}A$/HAuNS hydrogel were evaluated through 3D culture of HepG2 cells. After 48 h incubation, the cell viability of HepG2 cells in hydrogels was above 90% (Fig. 4d–g). In addition, hemolysis ration experiments were operated though incubated red blood cell (RBC) with $PC_{10}A$ hydrogel and $PC_{10}A$/HAuNS hydrogel (Fig. 4c). To serve as control groups, hemolysis ration experiments in ultrapure water and PBS were also investigated. The result showed that RBC in ultrapure water emerged completely hemolysis within 2 h. However, the hemolysis rates of $PC_{10}A$ hydrogel and $PC_{10}A$/HAuNS hydrogel were below 4% after incubation for 8 h. This result further demonstrated that $PC_{10}A$ hydrogel was promised to be applied as a safety drug carrier for biomedical application.

Hydrogel erosion and DOX release in vitro

$PC_{10}A$ hydrogel is a physical hydrogel formed by the coiled-coil P and A domains self-assembly, which can degrade slowly in PBS [39]. The erosion profile of 3% w/w $PC_{10}A$ hydrogel showed linear degradation behavior with time in the open aqueous solution system (Fig. 5a). At 37 °C in PBS, the accumulative release of a 3% w/w $PC_{10}A$ hydrogel was about 13% in 6 days. This result indicated that erosion was emerged on the surface rather than in whole bulk. In addition, the release of DOX from $PC_{10}A$/DOX/HAuNS hydrogels at different pH was evaluated. As shown in Fig. 5b, DOX was released rapidly in the first 12 h, and the release rate of DOX decreased gradually after 12 h. Compared with the DOX released from $PC_{10}A$/DOX/HAuNS hydrogels, the release rate and accumulative release of DOX from $PC_{10}A$/DOX

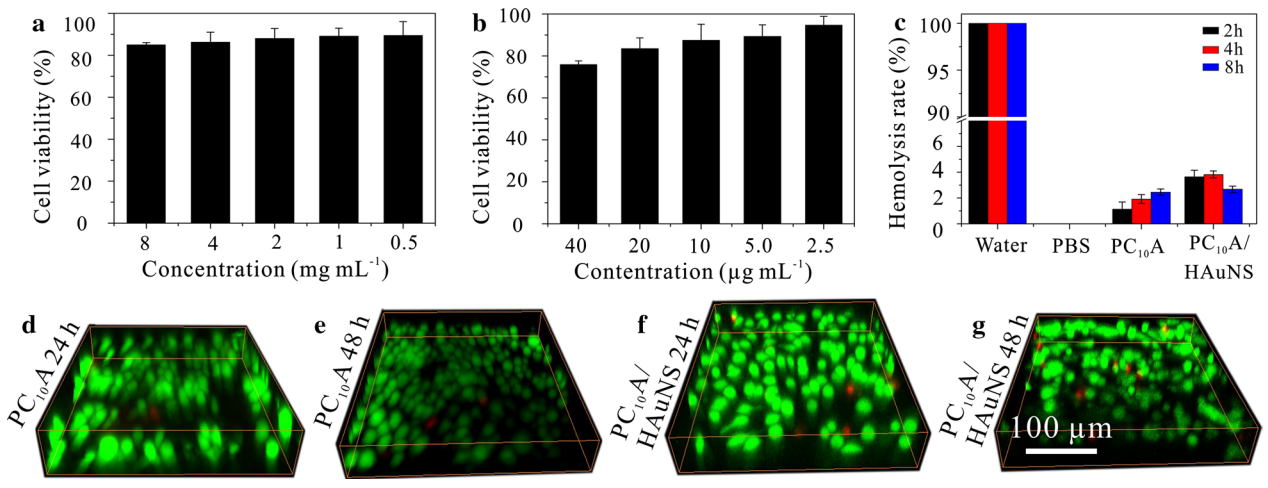

Fig. 4 Biocompatibility of $PC_{10}A$ nanogels and hemolysis ration of $PC_{10}A$ hydrogel. The cell viability of HepG2 cells incubated with different concentrations of $PC_{10}A$ nanogels (**a**) and HAuNS (**b**); **c** hemolysis ration of $PC_{10}A$ hydrogel and $PC_{10}A$/HAuNS hydrogel incubated with RBC for a series of time points (2, 4, and 8 h); **d**–**g** 3D cell culture of HepG2 cells in $PC_{10}A$ hydrogel (3% w/w) and $PC_{10}A$/HAuNS hydrogel ($PC_{10}A$: 3% w/w; HAuNS: 20 μg mL^{-1}) for 24 h and 48 h

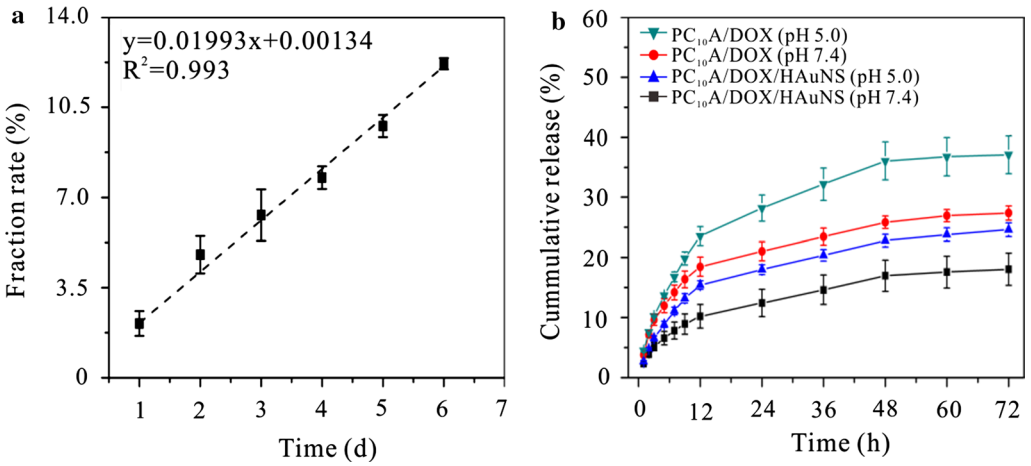

Fig. 5 Fraction rate of $PC_{10}A$ hydrogel (3% w/w) (**a**) and cumulative release of DOX from $PC_{10}A$/DOX hydrogel and $PC_{10}A$/DOX/HAuNS hydrogel (**b**) ($PC_{10}A$: 3% w/w; DOX: 0.8 mg mL^{-1}; HAuNS: 20 μg mL^{-1}) at different pH

hydrogels were faster and greater, which may be due to the existence of two forms of DOX in $PC_{10}A$/DOX/HAuNS hydrogels, one was directly embedded in the $PC_{10}A$ hydrogel, and the other was adsorbed on the surface of HAuNS nanoparticles in the $PC_{10}A$ hydrogel. Therefore, the DOX in $PC_{10}A$/DOX/HAuNS hydrogels could be released step by step for chemotherapy. Compared with chemically cross-linked hydrogel, the release rate of DOX released from physical $PC_{10}A$ hydrogel was faster. This is probably because the release of DOX from $PC_{10}A$ hydrogel was contributed by the degradation of $PC_{10}A$ hydrogel and diffusion. The release rate of DOX from $PC_{10}A$/DOX/HAuNS hydrogels in the acetate buffer of pH 5.0 was faster than that of in the PBS of pH 7.4, which was benefit for the drug release under acid microenvironment in tumor chemotherapy. Therefore, step-by-step release of DOX from $PC_{10}A$/DOX/HAuNS hydrogels could provide a new strategy for long-term chemotherapy of tumors.

Intratumoral retention experiment and drug distribution in vivo

To investigate the drug retardant capability of $PC_{10}A$ hydrogel, near infrared fluorescent dye IR783 encapsulated in the $PC_{10}A$/IR783 hydrogel was utilized to monitor drug accumulation in tumor and distribution in major organs. Two groups of HepG2 tumor xenograft male BALB/c nude mice were set up as models. $PC_{10}A$/IR783 hydrogel and free IR783 solution were respectively injected into the tumors with an equivalent IR783 dosage (40 μg mL^{-1}). The release routine of IR783 was monitored by a self-built wide-field fluorescence imaging system (Fig. 6a). It is clearly seen that the fluorescence intensity decayed rapidly at the first day and almost vanished after injection on day 6 in the control group injected with free IR783 solution. However, no obvious change of fluorescent intensity in the $PC_{10}A$/IR783 hydrogel positive group was observed on the third day, and a certain fluorescence signal of IR783 could still be seen on day 30. This result indicated that the release of IR783 of $PC_{10}A$/IR783 hydrogel in tumors presented a sustained release process. To obtain a clearer insight of the distribution about IR783 in different organs (heart, liver, spleen, lung, and kidney) and tumors, another two groups of mice were sacrificed at day 6 after injection of $PC_{10}A$/IR 783 hydrogel and free IR783 solution, respectively, and the fluorescence imaging of the main organs and tumors of the mice was measured. As shown in Fig. 6b, in the control group, almost no fluorescence signal was observed in the tumor and the main organs except in the liver. While IR783 in the $PC_{10}A$ hydrogel was mostly blocked at the site of the tumor. This result indicated that $PC_{10}A$ hydrogel could be used as a preeminent drug carrier for long term chemotherapy.

Combination of photothermal therapy and chemotherapy in vitro and in vivo

The therapeutic efficacies of $PC_{10}A$/HAuNS hydrogel, $PC_{10}A$/DOX hydrogel, and $PC_{10}A$/DOX/HAuNS hydrogel on HepG2 cells in vitro were evaluated. The therapeutic efficacy of blank $PC_{10}A$ hydrogel was used as a control. HepG2 cells embedded in $PC_{10}A$ hydrogel, $PC_{10}A$/HAuNS hydrogel, and $PC_{10}A$/DOX/HAuNS hydrogel were all irradiated with an 808 nm laser at the power density of 2.0 W cm^{-2} for 9 min. As shown in Fig. 7, cells in blank $PC_{10}A$ hydrogel and $PC_{10}A$/HAuNS hydrogel without laser irradiation were all survived well, revealing that blank $PC_{10}A$ hydrogel and $PC_{10}A$/

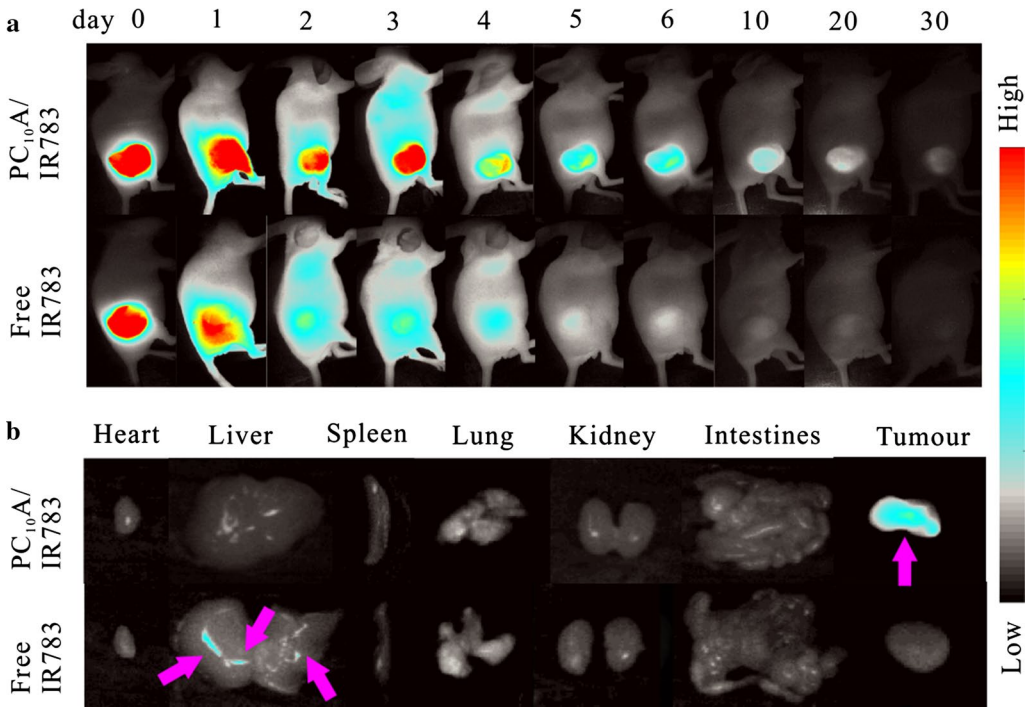

Fig. 6 **a** Fluorescence imaging of the BALB/c nude mice injected with $PC_{10}A$/IR783 hydrogel and IR783 solution ($PC_{10}A$: 3% w/w, IR783: 40 μg mL^{-1}) for different time intervals (day 0, 1, 2, 3, 4, 5, 6, 10, 20, and 30); **b** fluorescence imaging of the main organs (heart, liver, spleen, lung, and kidney) and tumors of the mice on day 6

HAuNS hydrogel without laser irradiation had no effect to HepG2 cells. Whereas more dead cells in $PC_{10}A$/DOX hydrogel and $PC_{10}A$/HAuNS hydrogel treated with laser irradiation were found. In addition, few living cells were observed in the $PC_{10}A$/DOX/HAuNS hydrogel treated with laser irradiation. These results demonstrated that neither $PC_{10}A$/HAuNS hydrogel treated with laser irradiation nor $PC_{10}A$/DOX hydrogel could effectively kill all HepG2 cells, and the combination of chemotherapy and photothermal therapy could completely kill HepG2 cells in the $PC_{10}A$/DOX/HAuNS hydrogel.

To further study anti-tumor efficacy of $PC_{10}A$/DOX/HAuNS hydrogel in vivo, the temperature changing of the HepG2 tumor injected with $PC_{10}A$/DOX/HAuNS hydrogel under laser irradiation ($\lambda = 808$ nm, 2.0 W cm^{-2}) was firstly measured. After exploring with the laser irradiation for 9 min, the temperature of the tumor reached up to 55.9 °C (Fig. 8a). While the temperature of the tumor injected with PBS only increased a little. These results suggested that the $PC_{10}A$/DOX/HAuNS hydrogel still presented excellent photothermal effect in vivo. Therefore, the $PC_{10}A$/DOX/HAuNS hydrogel is expected to be used as a photothermal agent for in vivo photothermal therapy of tumors.

Forty-two HepG2-tumor-bearing male mice were randomly divided into 7 groups: (1) PBS group, (2) laser irradiation alone group, (3) blank $PC_{10}A$ group, (4) free DOX group, (5) $PC_{10}A$/DOX hydrogel group, (6) $PC_{10}A$/HAuNS hydrogel group with laser irradiation, and (7) $PC_{10}A$/DOX/HAuNS group with laser irradiation ($n = 6$). The in vivo antitumor efficacies of multifunctional $PC_{10}A$/DOX/HAuNS hydrogel were tested through intratumoral injection. One mouse of each group was sacrificed for the tumor H&E stained histological section after treatment for 24 h to investigate the damage of tumor cells (Fig. 8b). Tumors injected with free DOX, $PC_{10}A$/DOX hydrogel, $PC_{10}A$/HAuNS hydrogel (laser+), and $PC_{10}A$/DOX/HAuNS hydrogel (laser+) exhibited mass cell apoptosis. While no obvious damage were observed in PBS group, blank $PC_{10}A$ hydrogel group, and laser irradiation alone group, indicating that $PC_{10}A$ hydrogel and transient laser had no damage to tumor cells. After 12 days of treatment, the tumors in each group showed different growth trends. The sizes of tumors injected with PBS, $PC_{10}A$ hydrogel, and laser irradiation alone groups kept remarkable expanding during this course, suggesting that blank $PC_{10}A$ hydrogel and the laser irradiation alone could not suppress HepG2 tumor growth. Compared with the PBS control group, free DOX solution and $PC_{10}A$/DOX hydrogel treatment groups delayed tumor growth. The sizes of tumors injected with $PC_{10}A$/DOX hydrogel

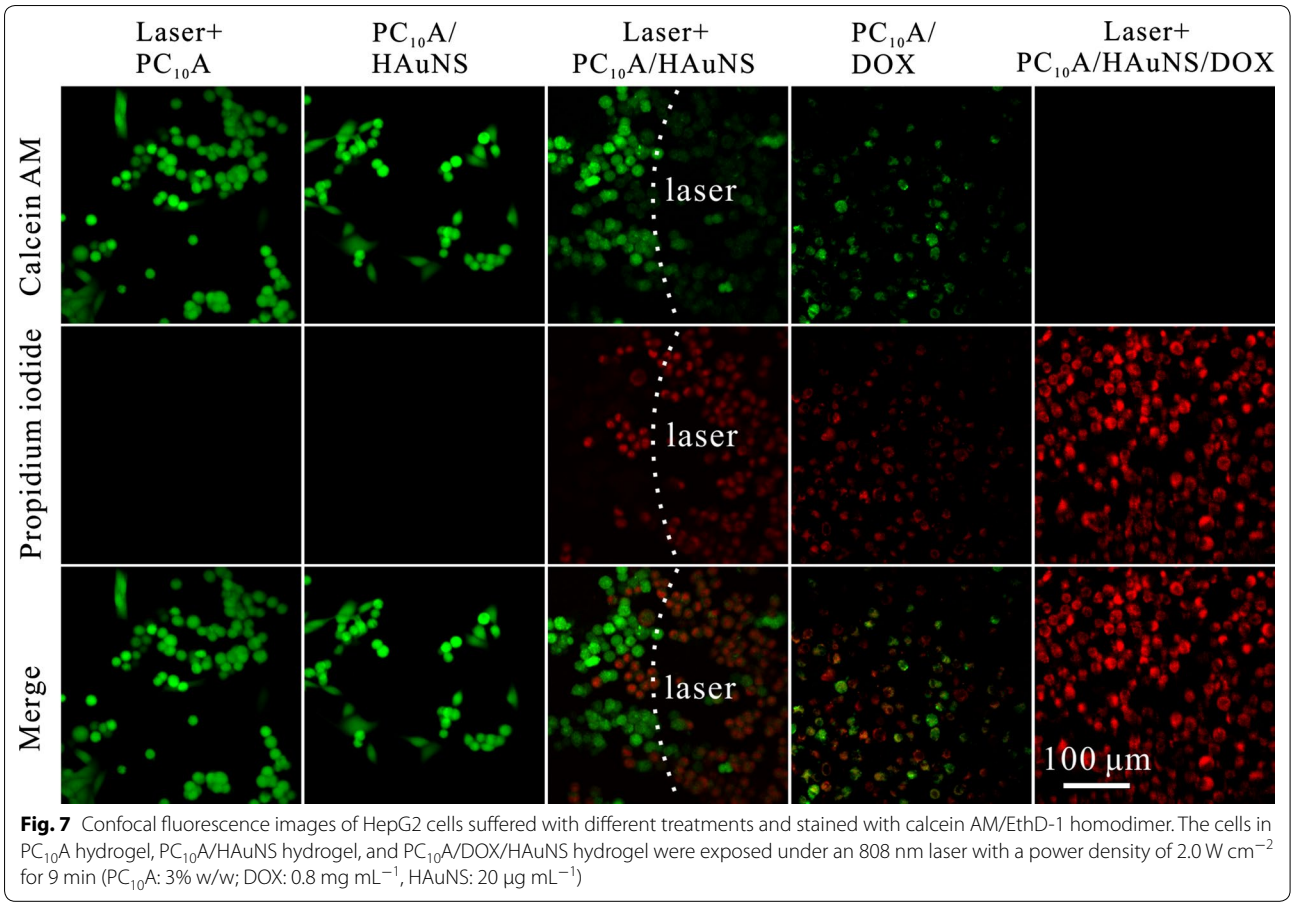

Fig. 7 Confocal fluorescence images of HepG2 cells suffered with different treatments and stained with calcein AM/EthD-1 homodimer. The cells in $PC_{10}A$ hydrogel, $PC_{10}A$/HAuNS hydrogel, and $PC_{10}A$/DOX/HAuNS hydrogel were exposed under an 808 nm laser with a power density of 2.0 W cm^{-2} for 9 min ($PC_{10}A$: 3% w/w; DOX: 0.8 mg mL^{-1}, HAuNS: 20 μg mL^{-1})

group were smaller than those of injected with free DOX solution. This is probably due to the sustained release of DOX from the $PC_{10}A$/DOX hydrogel and the rapid cleaning of free DOX during blood circulation. Notably, tumors injected with $PC_{10}A$/HAuNS hydrogel (laser+) and $PC_{10}A$/DOX/HAuNS hydrogel (laser+) scarred rapidly after treatment, which may be due to the hyperthermia caused by laser irradiation (Fig. 8b). In the group of $PC_{10}A$/HAuNS hydrogel (laser+), the sizes of tumors decreased sharply with time and then increased gradually. This is probably because pre-tumor inhibition was mainly due to the photothermal therapy of HAuNS in the hydrogel, and the recurrence was observed. This result indicated that photothermal therapy of HAuNS alone could not eliminate completely the tumor cells. As shown in Fig. 8c, d, the sizes of tumors treated with $PC_{10}A$/DOX/HAuNS hydrogels (laser+) decreased with time, even 80% tumors disappeared completely, which has been attributed to the combination of photothermal therapy and sustained chemotherapy. At the same time, body weights were recorded during the cure period (Fig. 8e), all of them have no obvious difference except for the free DOX solution group, which may attribute to the adverse effect caused by the flourish diffusion of free DOX.

Mice were sacrificed to collect blood and the major organs after 12 days post-injection. The blood was used for serum biochemistry assays and routine hematology analysis, and organs were utilized for H&E stain (Fig. 9). Related serum biochemical assay (Fig. 9a) included concentration test of alanine aminotransferase (ALT) and aspartate aminotransferase (AST). The routine hematology analysis contained red blood cell count (RBC), white blood cell count (WBC), blood platelet count (PLT), and hemoglobin (HGB) test. The values of AST and ALT of the free DOX group were all beyond normal range, suggesting that the heart and liver of these mice probably suffered from serious dysfunction. The content of RBC and HGB of the free DOX group also increased obviously, which may be due to hemolysis caused by free DOX. All the other index of the free DOX group also showed significant variation compared with the control group, meaning that free DOX were toxic to the mice ($n = 5$, $p < 0.05$). The index values of other groups were all in normal section, indicating that there was no obvious blood toxicity. In addition, the histological tissue slices of

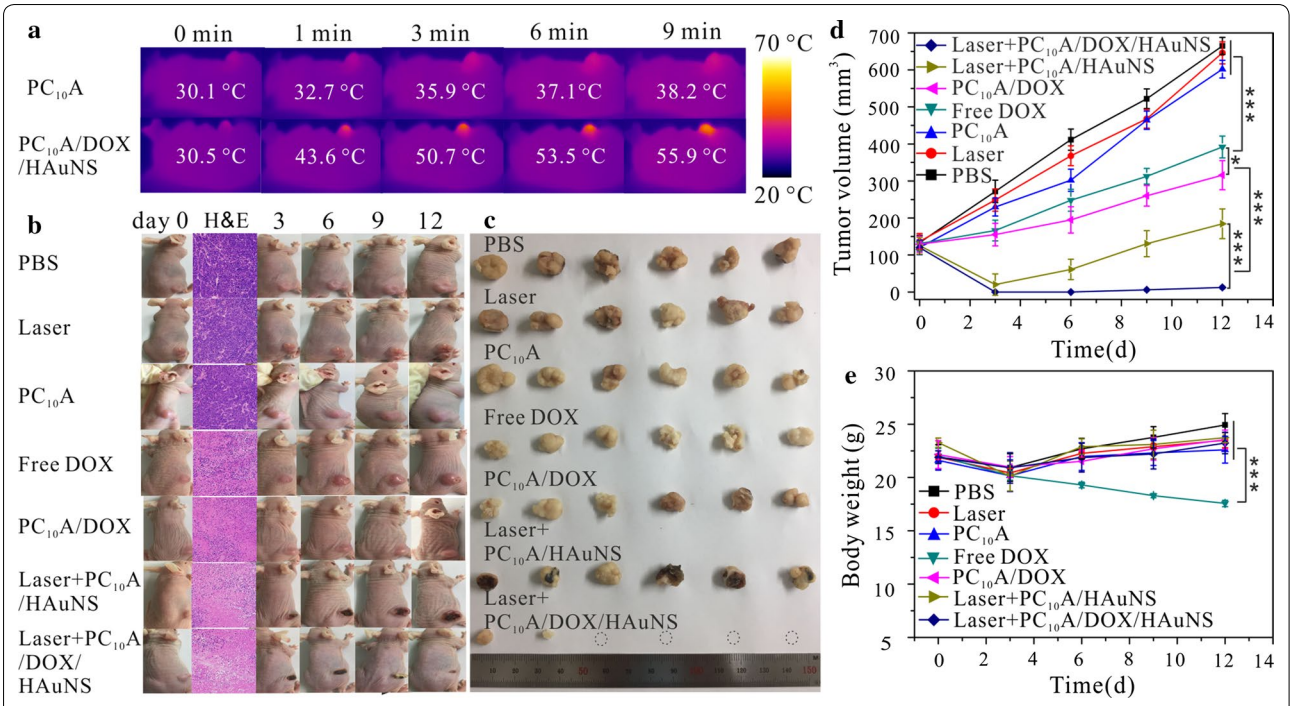

Fig. 8 Anti-tumor efficiency of $PC_{10}A$/DOX/HAuNS hydrogel in vivo. **a** Temperature changes of tumors after injected with $PC_{10}A$ hydrogel and $PC_{10}A$/DOX/HAuNS hydrogel (100 μL) at different period of irradiation with an 808 nm laser at power density of 2.0 W cm^{-2}; **b** photographs of the mice (H&E stained histological section of tumors after treatment for 1 day, the blue and pink indicated normal tissue cells and damaged tissue cells, respectively); **c** pictures of the tumors extracted from mice on day 12, **d** tumor volume and **e** body weight of the mice after treatment with PBS, laser irradiation, $PC_{10}A$ hydrogel, free DOX solution, $PC_{10}A$/DOX hydrogel, $PC_{10}A$/HAuNS hydrogel with laser, and $PC_{10}A$/DOX/HAuNS hydrogel with laser (808 nm, 2.0 W cm^{-2}, 9 min). n = 6, *p < 0.05, **p < 0.01, ***p < 0.001

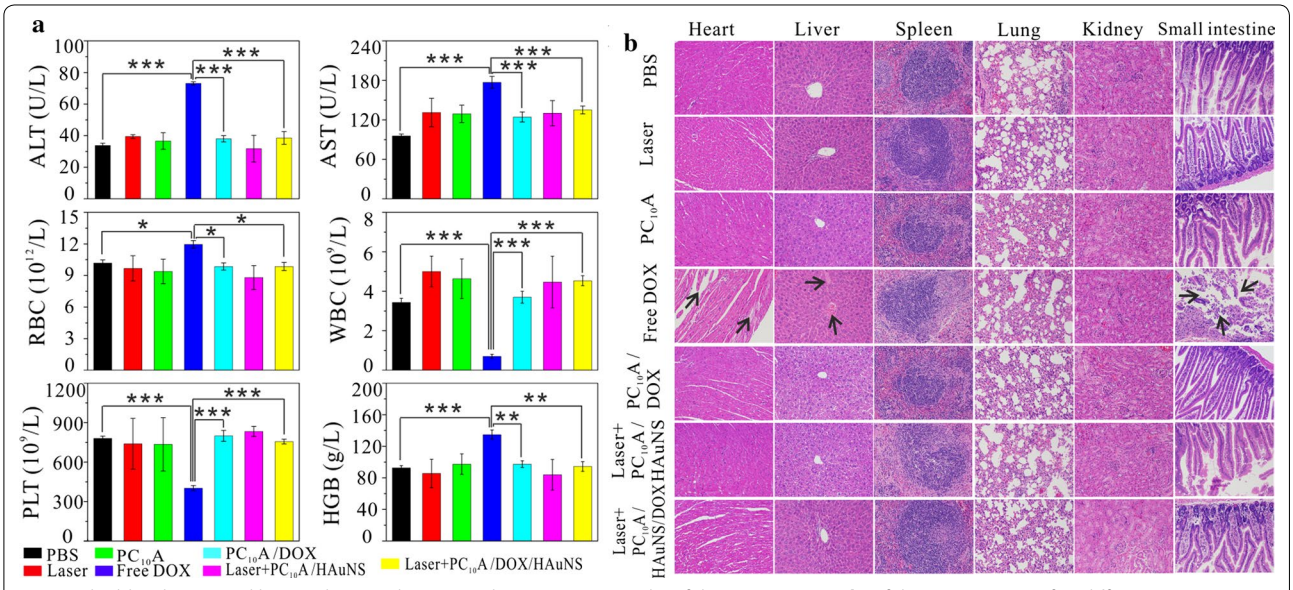

Fig. 9 The blood assay and hematology analysis (**a**) and H&E staining results of the major organs (**b**) of the BALB/c mice after different treatments. The arrows indicated damaged tissue cells. n = 6, *p < 0.05, **p < 0.01, and ***p < 0.001

major organs including heart, liver, spleen, lung, kidney and small intestine were also shown in Fig. 9b. Mice of the free DOX group exhibited some heart toxicity and led to severe inflammatory cells necrosis and gap enlarging. Simultaneously hyperemia bleeding and blood vessel congestion of the free DOX group appeared in hepatic sinus, and small intestinal villi distributed irregularly and seriously fell away. These results indicated that liver and small intestinal were also destructed partially. However, no obvious malformations were observed in other groups except for free DOX groups, suggesting that DOX encapsulated in $PC_{10}A$ hydrogel exhibited low systemic toxicity and were safe for in vivo applications.

Long-term tumor therapy and the recurrence rate in vivo

As we know, tumor recurrence is a tough hinder for the cancer therapy. To further evaluate the long-term therapy efficacies and recurrence rates of tumors, another three groups (n = 5) of mice were treated with $PC_{10}A$/DOX hydrogel, $PC_{10}A$/HAuNS hydrogel with laser irradiation, and $PC_{10}A$/DOX/HAuNS hydrogel with laser irradiation, respectively. When the tumor volume was exceeded 1000 mm^3, the mice were decided death [40]. Tumors were divided and took photographs at the end of the cure (Fig. 10a, b). As shown in the tumor volume curve and the survival curve (Fig. 10e, f), tumors injected with $PC_{10}A$/DOX hydrogel kept growth over time and appeared mass mortality in 30 days. This result indicated that the chemotherapy alone presented a weak tumor inhibition efficacy. The volume of tumors injected with $PC_{10}A$/HAuNS hydrogel (laser+) shrank quickly, but the volume of tumors began to gradually increase again on day 6. The survival rate descended radically in 70 days. These results showed that phototherapy alone could restrain the tumor in short time. In contrast, tumors treated with $PC_{10}A$/DOX/HAuNS hydrogels (laser+) were suppressed perfectly. The recurrence rate and survived rate of mice after 72 days treatment with $PC_{10}A$/DOX/HAuNS hydrogels (laser+) were 20% and 100%, respectively, which was superior to the single phototherapy or chemotherapy [41–43]. It is possible that a large number of tumor cells were first killed by photothermal treatment, and residual tumor cells were suppressed and eliminated by the DOX sustained releasing from $PC_{10}A$/DOX/HAuNS hydrogels. Interestingly, on day 72, there were

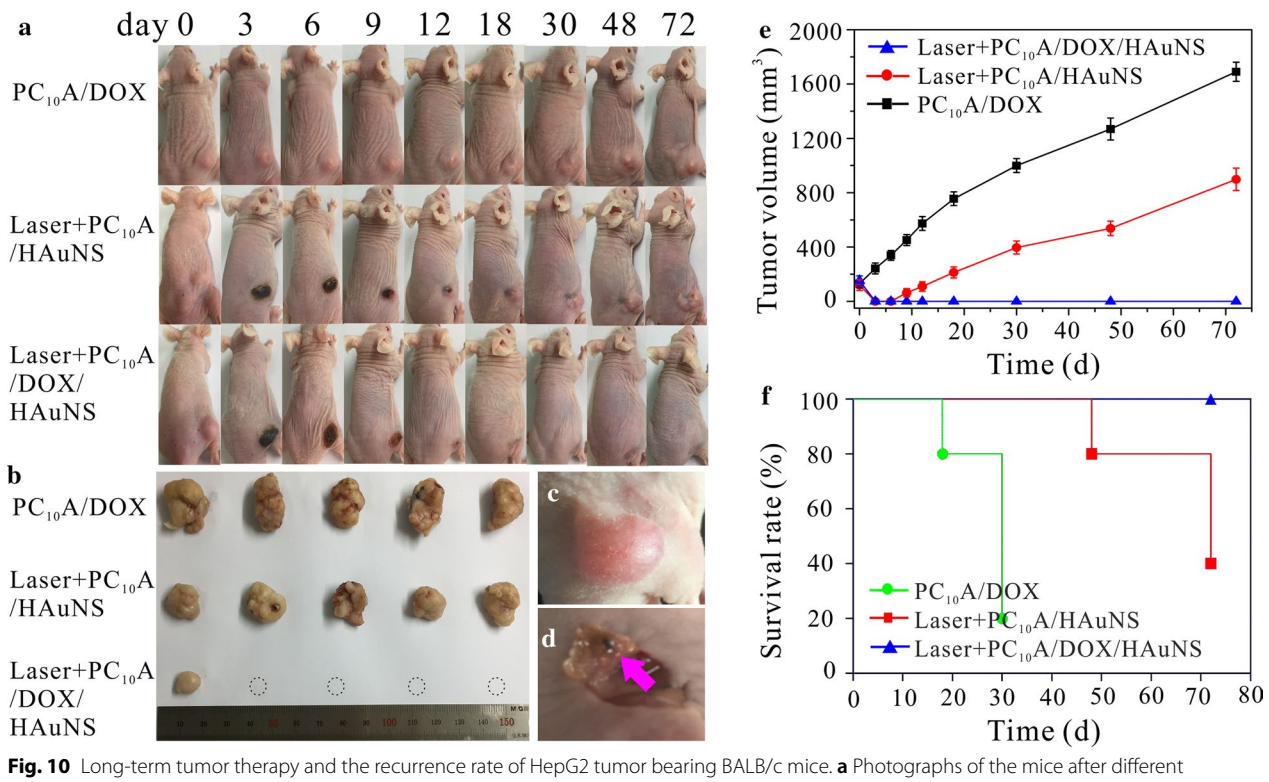

Fig. 10 Long-term tumor therapy and the recurrence rate of HepG2 tumor bearing BALB/c mice. **a** Photographs of the mice after different treatment; **b** pictures of the tumors extracted from mice on day 72; Pictures of tumor before (**c**) and after (**d**) treatment with $PC_{10}A$/DOX/HAuNS hydrogel on day 72 (There were still some $PC_{10}A$/DOX/HAuNS hydrogels in the tumor site); Tumor volume (**e**) and survival rate (**f**) of the mice after treatment with PBS, laser irradiation, $PC_{10}A$ hydrogel, free DOX solution, $PC_{10}A$/DOX hydrogel, $PC_{10}A$/HAuNS hydrogel with laser, and $PC_{10}A$/DOX/HAuNS hydrogel with laser (808 nm, 2.0 W cm^{-2}, 9 min)

still some $PC_{10}A$/DOX/HAuNS hydrogels in the tumor site of mice treated with $PC_{10}A$/DOX/HAuNS hydrogels (laser+) were found (Fig. 10c, d), but the volumes were smaller than those of the pre-injection hydrogel. This result demonstrated that $PC_{10}A$/DOX/HAuNS hydrogels could slowly degrade in vivo and sustained release of DOX for long-term chemotherapy. Therefore, this injectable $PC_{10}A$/HAuNS/DOX hydrogel is beneficial to the development of combined photothermal therapy and long-term chemotherapy of tumors.

Conclusion

In summary, we have developed a simple method to prepare the injectable $PC_{10}A$/DOX/HAuNS hydrogel based on the polypeptide $PC_{10}A$ and HAuNS for chemo-photothermal therapy of HepG2 tumor. Hybrid $PC_{10}A$/DOX/HAuNS nanoparticles were first prepared through self-assembled layer-by-layer, and multifunctional $PC_{10}A$/DOX/HAuNS hydrogels were prepared through "dissolving" the hybrid $PC_{10}A$/DOX/HAuNS nanoparticles in the $PC_{10}A$ hydrogel. The rheological properties of $PC_{10}A$/DOX/HAuNS hydrogel were tuned by simply changing the concentrations of $PC_{10}A$ and HAuNS. Excitingly, this multifunctional $PC_{10}A$/DOX/HAuNS hydrogel could pass 0.25 mm diameter needle without clogging. The results of photothermal effect showed that HAuNS in the $PC_{10}A$/DOX/HAuNS hydrogel still possessed excellent photothermal efficiency and photothermal stability. The results of in vitro and in vivo toxicity showed that the $PC_{10}A$/DOX/HAuNS hydrogel was non-toxic. Finally, the results of in vitro and in vivo treatment exhibited that the combined chemotherapy and photothermal therapy of $PC_{10}A$/DOX/HAuNS hydrogels could significantly improve the therapeutic effect. Therefore, these results reported here provide a new strategy for sustained chemo-photothermal therapy.

Supplementary information

Supplementary information accompanies this paper at https://doi.org/10.1186/s12951-019-0532-9.

Additional file 1. Additional figures.

Abbreviations

HAuNS: hollow gold nanoshells; DOX: doxorubicin Hydrochloride; IPTG: isopropyl-β-D-thiogalactoside; Ni-NTA: nickelnitrilotriacetic acid; $HAuCl_4 \cdot 3H_2O$: gold chloride trihydrate; PVP: polyvinylpyrrolidone; calcein-AM: calcein acetoxymethyl ester; WBC: white blood cell; RBC: red blood cell; HGB: hemoglobin; PLT: platelet; ALT: alanine aminotransferase; AST: aspartate aminotransferase; PTT: photothermal therapy; G′: storage moduli; G″: loss moduli.

Acknowledgements

The authors thank the Analytical and Testing Center (HUST), the Research Core Facilities for Life Science (HUST) and the Center for Nanoscale Characterization & Devices (CNCD) at WNLO of HUST for the help of measurement.

Authors' contributions

RMJ, JY, DHZ, XLH and CQL performed experiments and acquired the data. RMJ and JY contributed equally to this work and should be considered as co-first authors. YDZ, ZYY and BL designed experiment and give the intellectual input. All authors read and approved the final manuscript.

Funding

This work was supported by the National Key Research and Development Program of China (2017YFA0700501), the National Natural Science Foundation of China (Grant Nos. 81771878, 81871414), the China Postdoctoral Science Foundation (2017M612462), the Fundamental Research Funds for the Central Universities (Hust: 2016YXMS253, 2017KFXKJC002, 2018KFYXKJC048), and the Opening Project of Key Laboratory of Optoelectronic Chemical Materials and Devices, Ministry of Education, Jianghan University (JDGD-201709).

Availability of data and materials

All data generated or analyzed during this study are included in this published article (and its additional files).

Ethics approval and consent to participate

All animal experiments were approved by the Animal Experimental Ethics Committee of Huazhong University of Science and Technology.

Consent for publication

All authors agree to publish this manuscript.

Competing interests

The authors declare that they have no competing interests.

Author details

[1] Britton Chance Center for Biomedical Photonics at Wuhan National Laboratory for Optoelectronics-Hubei Bioinformatics & Molecular Imaging Key Laboratory, Collaborative Innovation Center for Biomedical Engineering, College of Life Science and Technology, Huazhong University of Science and Technology, Wuhan 430074, Hubei, People's Republic of China. [2] Key Laboratory of Biomedical Photonics (HUST), Ministry of Education, Huazhong University of Science and Technology, Wuhan 430074, Hubei, People's Republic of China. [3] Cancer Center, Union Hospital, Tongji Medical College, Huazhong University of Science and Technology, Wuhan 430022, Hubei, People's Republic of China.

Received: 8 July 2019 Accepted: 10 September 2019
Published online: 17 September 2019

References

1. Zhou ZJ, Yan Y, Wang L, Zhang Q, Cheng YY. Melanin-like nanoparticles decorated with an autophagy-inducing peptide for efficient targeted photothermal therapy. Biomaterials. 2019;203:63–72.
2. Cheng L, Zhang FR, Wang SH, Pan XT, Han SC, Liu S, Ma JJ, Wang HY, Shen HY, Liu HY, Yuan QP. Activation of prodrugs by NIR-triggered release of exogenous enzymes for locoregional chemo-photothermal therapy. Angew Chem Int Ed. 2019;58:7728–32.
3. Jung HL, Verwilst P, Sharma A, Shin J, Sessler JL, Kim JS. Organic molecule-based photothermal agents: an expanding photothermal therapy universe. Chem Soc Rev. 2018;47:2280–97.
4. Dong Q, Wang XW, Hu XX, Xiao LQ, Zhang L, Song LJ, Xu ML, Zou YX, Chen L, Chen Z, Tan WH. Simultaneous application of photothermal therapy and an antiinflammatory prodrug using pyrene–aspirin-loaded gold nanorod graphitic nanocapsules. Angew Chem. 2018;130:183–7.
5. Manivasagan P, Nguyen VT, Jun SW, Hoang G, Mondal S, Kim H, Doan M, Kim J, Kim CS, Oh J. Anti-EGFR antibody conjugated thiol chitosan-layered gold nanoshells for dual-modal imaging-guided cancer combination therapy. J Control Release. 2019;08:007.
6. You Q, Sun Q, Yu M, Wang JP, Wang SY, Liu L, Cheng Y, Wang YD, Song YL, Tan FP, Li N. BSA — bioinspired gadolinium hybrid-functionalized hollow gold nanoshells for NIRF/PA/CT/MR quadmodal diagnostic imaging-guided photothermal/photodynamic cancer therapy. ACS Appl Mater Interfaces. 2017;9:40017–30.

7. Xue P, Yang RH, Sun LH, Li Q, Zhang L, Xu ZG, Kang YJ. Indocyanine green-conjugated magnetic prussian blue nanoparticles for synchronous photothermal/photodynamic tumor therapy. Nano-Micro Lett. 2018;10:74.
8. He LZ, Nie TQ, Xia XJ, Liu T, Huang YY, Wang XJ, Chen TF. Designing bioinspired 2D $MoSe_2$ nanosheet for efficient photothermal-triggered cancer immunotherapy with reprogramming tumor-associated macrophages. Adv Funct Mater. 2019;190:1240.
9. Adams S, Zhang JZ. Unique optical properties and applications of hollow gold nanospheres (HGNs). Coord Chem Rev. 2016;320:18–37.
10. Zhou JL, Wang ZH, Li QP, Liu F, Du YZ, Yuan H, Hu FQ, Wei YH, You J. Hybridized doxorubicin-Au nanospheres exhibit enhanced near-infrared surface plasmon absorption for photothermal therapy applications. Nanoscale. 2015;7:5869–83.
11. Han S, Park YJ, Park EJ, Kim YH. T98G cell death induced by photothermal treatment with hollow gold nanoshell-coupled silica microrods prepared from *Escherichia coli*. ACS Appl Mater Interfaces. 2019;11(9):8831–7.
12. Li SW, Liu YX, Rui YL, Tang LP, Achilefu S, Gu YQ. Dual target gene therapy to EML4-ALK NSCLC by a gold nanoshell-based system. Theranostics. 2018;8(10):2621.
13. Chen WR, Adams RL, Higgins AK, Bartels KE, Nordquist RE. Photothermal effects on murine mammary tumors using indocyanine green and an 808-nm diode laser: an in vivo efficacy study. Cancer Lett. 1996;98:169–73.
14. Tang JL, Zhang RR, Guo MY, Shao LH, Liu Y, Zhao YL, Zhang SJ, Wu Y, Chen CY. Nucleosome-inspired nanocarrier obtains encapsulation efficiency enhancement and side effects reduction in chemotherapy by using fullerenol assembled with doxorubicin. Biomaterials. 2018;167:205–15.
15. Mittra I, Pal K, Pancholi N, Shaikh A, Rane B, Tidke P, Kirolikar S, Khare NK, Agrawal K, Nagare H, Nair NK. Prevention of chemotherapy toxicity by agents that neutralize or degrade cell-free chromatin. Ann Oncol. 2017;28:2119–27.
16. He QJ, Guo SG, Qian ZY, Chen XY. Development of individualized anti-metastasis strategies by engineering nanomedicines. Chem Soc Rev. 2015;44:6258–86.
17. Jiang TY, Wang T, Li T, Ma Y, Shen SY, He BF, Mo R. Enhanced transdermal drug delivery by transfersome-embedded oligopeptide hydrogel for topical chemotherapy of melanoma. ACS Nano. 2018;12:9693–701.
18. Sun B, Taha MS, Ramsey B, Torregrosa-Allen S, Elzey BD, Yeo Y. Intraperitoneal chemotherapy of ovarian cancer by hydrogel depot of paclitaxel nanocrystals. J Control Release. 2016;235:91–8.
19. Zhao JL, Li JL, Zhu CP, Hu F, Wu HY, Man XH, Li ZS, Ye CQ, Zou DW, Wang SG. Design of phase-changeable and injectable alginate hydrogel for imaging-guided tumor hyperthermia and chemotherapy. ACS Appl Mater Interfaces. 2018;10:3392–404.
20. Hu CH, Liu XY, Ran W, Meng J, Zhai YH, Zhang PC, Yin Q, Yu HJ, Zhang ZW, Li YP. Regulating cancer associated fibroblasts with losartan-loaded injectable peptide hydrogel to potentiate chemotherapy in inhibiting growth and lung metastasis of triple negative breast cancer. Biomaterials. 2017;144:60–72.
21. Hamidi M, Azadi A, Rafiei P. Hydrogel nanoparticles in drug delivery. Adv Drug Deliv Rev. 2008;60:1638–49.
22. Johnsona CT, Wroea JA, Agarwalb R, Martinb KE, Guldbergb RE, Donland RM, Westbladee LF, García AJ. Hydrogel delivery of lysostaphin eliminates orthopedic implant infection by staphylococcus aureus and supports fracture healing. Proc Natl Acad Sci USA. 2018;115:E4960–9.
23. Qi YQ, Min H, Mujeeb A, Zhang YL, Han XX, Zhao X, Anderson GJ, Zhao Y, Nie GJ. Injectable hexapeptide hydrogel for localized chemotherapy prevents breast cancer recurrence. ACS Appl Mater Interfaces. 2018;10:6972–81.
24. Bastiancicha C, Biancoa J, Vanvarenberga K, Ucakara B, Joudioub N, Gallezb B, Bastiatc G, Lagarcec F, Préata V, Danhiera F. Injectable nanomedicine hydrogel for local chemotherapy of glioblastoma after surgical resection. J Control Release. 2017;264:45–54.
25. Majumder P, Baxa U, Walsh STR, Schneider JP. Design of a multicompartment hydrogel that facilitates timeresolved delivery of combination therapy and synergized killing of glioblastoma. Angew Chem. 2018;130:15260–4.
26. Kim DY, Kwon DY, Kwon JS, Park JH, Park SH, Oh HJ, Kim JH, Min BH, Park K, Kim MS. Synergistic anti-tumor activity through combinational intratumoral injection of an in situ injectable drug depot. Biomaterials. 2016;85:232–45.
27. Zhang YS, Khademhosseini A. Advances in engineering hydrogels. Science. 2017;356:3627.
28. Grozea CM, Walker GC. Approaches in designing non-toxic polymer surfaces to deter marine biofouling. Soft Matter. 2009;5:4088–100.
29. Yu YB. Coiled-coils: stability, specificity, and drug delivery potential. Adv Drug Deliv Rev. 2002;54:1113–29.
30. Lee HJ, Liu Y, Zhao J, Zhou M, Bouchard RR, Mitcham T, Wallace M, Stafford RJ, Li C, Gupta S, Melancon MP. In vitro and in vivo mapping of drug release after laser ablation thermal therapy with doxorubicin-loaded hollow gold nanoshells using fluorescence and photoacoustic imaging. J Control Release. 2013;172:152–8.
31. Wang L, Yuan YY, Lin SD, Huang JS, Dai J, Jiang Q, Cheng D, Shuai XT. Photothermo-chemotherapy of cancer employing drug leakage-free gold nanoshells. Biomaterials. 2016;78:40–9.
32. Zhao DH, Yang J, Xia RX, Yao MH, Jin RM, Zhao YD, Liu B. High quantum yield Ag_2S quantum dot@polypeptide-engineered hybrid nanogels for targeted second near-infrared fluorescence/photoacoustic imaging and photothermal therapy. Chem Commun. 2018;54:527–30.
33. Yao MH, Yang J, Song JT, Zhao DH, Du MS, Zhao YD, Liu B. Directed self-assembly of polypeptide-engineered physical microgels for building porous cell-laden hydrogels. Chem Commun. 2014;50:9405–8.
34. Schwartzberg AM, Olson TY, Talley CE, Zhang JZ. Synthesis, characterization, and tunable optical properties of hollow gold nanospheres. J Phys Chem B. 2006;110:19935–44.
35. Roper DK, Ahn W, Hoepfner M. Microscale heat transfer transduced by surface plasmon resonant gold nanoparticles. J Phys Chem C. 2007;111:3636–41.
36. Appel EA, del Barrio J, Loh XJ, Oren AS. Supramolecular polymeric hydrogels. Chem Soc Rev. 2012;41(18):6195–214.
37. Huang G, Zhang HH, Liu Y, Liu YL, Chang HJ, Zhang HW, Song HZ, Xu DH, Shi TF. Strain hardening behavior of poly (vinyl alcohol)/borate hydrogels. Macromolecules. 2017;50(5):2124–35.
38. Guvendiren M, Lu HD, Burdick JA. Shear-thinning hydrogels for biomedical applications. Soft Matter. 2012;8:260–72.
39. Shen W, Zhang K, Kornfield JA, Tirrell DA. Tuning the erosion rate of artificial protein hydrogels through control of network topology. Nat Mater. 2006;5:153–8.
40. Lyu Y, Fang Y, Miao QQ, Zhen X, Ding D, Pu K. Intraparticle molecular orbital engineering of semiconducting polymer nanoparticles as amplified theranostics for in vivo photoacoustic imaging and photothermal therapy. ACS Nano. 2016;10:4472–81.
41. Li LY, Zhou YM, Gao RY, Liu XC, Du HH, Zhang JL, Ai XC, Zhang JP, Fu LM, Skibsted LH. Naturally occurring nanotube with surface modification as biocompatible, target-specific nanocarrier for cancer phototherapy. Biomaterials. 2019;190:86–96.
42. Mou QB, Ma Y, Zhu XY, Yan DY. A small molecule nanodrug consisting of amphiphilic targeting ligand–chemotherapy drug conjugate for targeted cancer therapy. J Control Release. 2016;230:34–44.
43. Luo LY, Bian YH, Liu YP, Zhang XW, Wang ML, Xing SS, Lei L, Gao DW. Combined near infrared photothermal therapy and chemotherapy using gold nanoshells coated liposomes to enhance antitumor effect. Small. 2016;12(30):4103–12.

Publisher's Note